J Mater Sci (2015) 50:1688–1700
DOI 10.1007/s10853-014-8730-1

Antibacterial efficacy, corrosion resistance, and cytotoxicity studies of copper-substituted carbonated hydroxyapatite coating on titanium substrate

Yong Huang · Xuejiao Zhang · Ranlin Zhao · Huanhuan Mao · Yajing Yan · Xiaofeng Pang

Received: 6 October 2014 / Accepted: 17 November 2014 / Published online: 25 November 2014

Abstract This work elucidated the antibacterial efficacy, corrosion resistance, and cytotoxicity of electroplated copper-substituted hydroxyapatite (CuHAP) coating on titanium (Ti). The fabricated CuHAP coatings were characterized by scanning electron microscopy, energy-dispersive X-ray analysis spectroscopy, Fourier transform infrared spectroscopy, and X-ray diffraction studies. The CuHAP coating had needle-like apatite crystals, the doping of Cu^{2+} into HAP reduced porosity, and the coating became denser. The CuHAP crystals were carbonated with a few of Cu^{2+} incorporation (about 0.80 wt%). The Cu^{2+} ions were homogenously deposited into HAP films. Potentiodynamic polarisation test revealed that the CuHAP coating provided good barrier characteristics and achieved superior corrosion protection for Ti substrates. The in vitro antibacterial activity of as-prepared CuHAP coating was evaluated against *Escherichia coli* and was found to be effectively high against bacterial colonization. Bioactivity test conducted by soaking the coatings in simulated body fluid demonstrated that CuHAP coating can quickly induce bone-like apatite nucleation and growth. In vitro biocompatibility tests, MTT, were employed to assess the cytotoxicity of Cu-HAP coating with osteoblast-like MC3T3-E1 cells. The obtained HAP coating doped with a low content of Cu^{2+} exhibited good cytocompatibility and had no toxicity toward MC3T3-E1.

Introduction

Titanium (Ti) and its alloys are used extensively for medical implants in oral and orthopedic, due to their low density, high strength, non-toxicity, and superior corrosion resistance [1]. To further stimulate the bone-bonding ability, metallic implants are generally coated with osteoconductive biomaterials, such as hydroxyapatite (HAP, $Ca_{10}(PO_4)_6(OH)_2$) bioceramic [2, 3]. Artificial synthetic HAP is extremely similar to the inorganic part of bones and the dentine of teeth, and it is non-toxic within any quantity and osteoconductive [4]. HAP has been commonly designed as a coating material for metallic implants owing to its superior cytocompatibility, ability to stimulate cellular functions, and osteoconductivity [5].

However, the successful application of HAP has several disadvantages which also involve the lack of antibacterial activity that impacts its long-term stability and gives rise to implant failures [6]. This induces the increased risk of bacterial adherence and colonization of the metallic implants coated with HAP [7]. This morbidity of implant material revolved infections is hard to treat. Consequently, the introduction of antibacterial activity into HAP is used to ensure the success of the implants covered with HAP [8]. In recent years, the doping of biological materials with some metallic antibacterial agents (such as Cu^{2+}, Ag^{+}, Ti^{4+}, and Zn^{2+}) is more appropriate because they show

Y. Huang · X. Zhang
College of Lab Medicine, Hebei North University, Zhangjiakou 075000, China

Y. Huang (✉) · R. Zhao · H. Mao · Y. Yan · X. Pang
Institute of Life Science and Technology, University of Electronic Science and Technology of China, Chengdu 610054, China
e-mail: xfpang@aliyun.com

X. Pang
International Centre for Materials Physics, Chinese Academy of Science, Shenyang 110015, China

antimicrobial activity at the site of implant materials and they are not cytotoxic at low concentrations [9–12]. Besides its antimicrobial activity, Cu is an essential trace element for mammalian life [10, 13], and it stimulates the activity of several enzymes and plays a role in the cross-linking of collagen and elastin of bones [10, 14].

Several methods have been used to synthesize the HAP coating on metallic implants [1], such as electrochemical deposition, biomimetic coating, hot isostatic pressing, pulsed laser ablation, sputter coating, dynamic mixing, ion-beam-assisted deposition, sol–gel, thermal spraying, dip coating, and plasma spraying process. Among the methods listed, plasma spraying is the only technique which is approved by the Food and Drug Administration (FDA) [1]. However, this method poses several defects: (1) it requires excessively high temperatures and costly equipments; (2) it does not elicit carefully organized growth, so the mineral initiates in non-specific sites; (3) it cannot coat porous surfaces or include bioactive agents; and (4) the poor substrate-coating bond constantly culminates in many clinical problems [3]. In this sense, electrolytic deposition (ED) has proven to be among the most versatile methods for the synthesis of ion-substituted HAP composite coatings [15, 16], with characteristics superior to conventional deposition techniques (low process temperature, low-cost equipment, probability of fabricating onto porous substrates of complicated shapes, and simple control of coating properties). There are several reports on the individual substitution of several ions such as Sr, Mg, Mn, Ag, Zn, Na, and F into HAP coating [17–23]; however, to the best of our knowledge, there are very limited reports concerning the electrodeposition of Cu^{2+}-substituted HAP coating on metallic substrate. Hence, in this work, we will report the preparation of CuHAP coatings to investigate their advantages in terms of their antibacterial efficacy, corrosion resistance, and cytotoxicity in vitro.

In the present study, we incorporate Cu^{2+} into electrodeposited HAP coatings to enhance the antibacterial efficacy, corrosion resistance, and cell–biomaterial interactions. The crystallinity, phase purity, level of ionic substitution, and coating morphology were evaluated by X-ray diffraction (XRD), scanning electron microscopy (SEM), energy-dispersive spectroscopy (EDS), and Fourier transmission infrared spectroscopy (FTIR). The in vitro antibacterial effect of the CuHAP coating was evaluated using *Escherichia coli*. Simulated body fluid (SBF) researches up to 10 days were conducted in order to provide an indication of the bioactivity of the Cu-substituted samples. Furthermore, a MTT assay was performed to assess the viability of cultured MC3T3-E1 osteoblast precursor cells seeded on pure and Cu-substituted HAP coatings.

Materials and methods

Preparation of Cu^{2+}-substituted HAP coating

Commercially pure Ti plates (99.9 % purity, Non-Ferrous Metals, Ltd., Baoji, China) of 10 × 10 × 1 mm^3 size were designed as the substrates. The pretreatment of the substrate surface was performed according to the procedures described earlier [19–21]. ED was carried out using a LK2005A electrochemical workstation (Tianjin, China). An ED apparatus with saturated calomel electrode, Ti plate, and platinum sheets were designated as the reference, working, and auxiliary electrodes, respectively. The analytical-grade calcium nitrate tetrahydrate ($Ca(NO_3)_2 \cdot 4H_2O$), cupric nitrate ($Cu(NO_3)_2 \cdot 3H_2O$), and ammonium dihydrogen phosphate ($NH_4H_2PO_4$) were adopted as the sources for Ca, Cu, and P, respectively. The electrolyte was prepared with a theoretical Ca/P ratio of 1.67 for apatite. CuHAP coating was conducted in an electrolyte composed of 4.2×10^{-2} M $Ca(NO_3)_2 \cdot 4H_2O$, 2.5×10^{-2} M $NH_4H_2PO_4$, and 2.5×10^{-3} M $Cu(NO_3)_2 \cdot 3H_2O$ under the following parameters [19]: pH 4.4 ± 0.5, 1 mA cm^{-2} current density, 15–25 min, and 65 ± 0.5 °C. After deposition, the samples were immersed in 1 M NaOH solution at 65 °C for approximately 1 h, gently rinsed with distilled water, and dried in an oven at 65 °C for 2 h. The dried films were sintered at 250 °C for 2 h in air. The hot specimens were cooled down slowly in the oven to decrease the stress. For comparison, pure HAP coating was designated as control.

Sample characterisation

The morphologies and elemental analysis of the as-deposited coatings (HAP and CuHAP) were identified using a SEM (JEOL JSM-7500F, Japan), equipped with energy-dispersive X-ray analysis spectroscopy (EDAX) (GENESIS 2000 XMS). XRD (BEDE D1 SYSTEM, with Cu Ka radiation operated at 35 mA and 35 kV) was used to analyze the crystalline phase structure of the as-synthesized coatings. The XRDs were taken at 2θ angle range from 20° to 60° and scanned at a step size of 0.06° s^{-1}. The functional groups present in the as-synthesized coatings were analyzed by Nicolet 670 FTIR Spectrometer (USA) over the range from 400 to 4000 cm^{-1} with a number of scans 64 and resolution 4 cm^{-1}. The specimens were prepared by mixing 0.001 g of the deposit powder (scraped off from the Ti surface) together with 0.1 g of KBr to make a pellet.

Potentiodynamic polarisation assay

Potentiodynamic polarisation test was performed according to the procedures described earlier [19–21], which was based on previously established tests [15, 24, 25].

Antimicrobial activity test

E. coil microorganism was employed to analyze the antimicrobial activity. Antimicrobial activity of the CuHAP coating with *E. coil* was measured by the plate-counting method. Before the test, all samples were sterilized at 121 °C for 20 min by autoclave. The concentration of bacterial solution was adjusted to 10^5 CFU/ml with sterilized PBS, then 30 µl of bacterial solutions were dripped separately on the surface of the samples, and the samples were covered with an aseptic polyethylene film. After the samples were incubated with *E. coil* at 37 °C for 24 h, each sample was placed into the tube with 10 ml sterilized PBS (pH 7.2), followed by shaking at 200 rm for 5 min, and 100 µl of the shaken bacterial solutions were then spread evenly on Luria-Bertani medium agar plates. The incubation period was conducted in a thermostat, at 37 °C for 24 h, and then counted the visible cells of each plate by quantifying the CFUs. Each test was performed in triplicate, and the witness test also be applied as a control group. Hence, antimicrobial ratio (K) of the coatings was calculated using the formula [8]:

$$K = \frac{A - B}{A} \times 100,$$

where A was the average number of colonies in the control and B was the average number of bacterial colonies in the CuHAP or HAP coating.

In vitro biomineralization of the deposited coating

The Ti substrates coated with CuHAP were soaked in SBF to study the in vitro biomineralization behavior. The SBF had ionic composition similar to that of human plasma [26]. SBF solution was prepared in accordance with ISO 23317:2007 by the procedure proposed by Kokubo et al. [26], as shown in Table 1. The soaking periods were 10 days. The SBF was renewed every 24 h with the temperature being maintained at 310 K. SBF assay was performed according to the procedures described earlier [19].

Cytotoxicity test

MC3T3-E1 osteoblast-like cells, from mouse skull (West China School of Medicine), were cultured at 37 °C in a humidified 5 % CO_2 atmosphere in standard culture medium, Dulbecco's Modified Eagle Medium (DMEM, GIBCO), which consisted of α-minimal essential medium (Hyclone), supplemented with 10 % fetal bovine serum (HyClone), and 1 % penicillin/streptomycin (GIBCO). To evaluate the cytotoxicity of CuHAP coating, MC3T3-E1 cells with 2×10^4 cells ml^{-1} densities were seeded onto the samples. Cell adhesion test and MTT assay were performed according to the procedures described earlier [19, 21, 22], which were based on previously established tests [15, 18].

Statistical analysis

Statistical significance analysis was carried out using SPSS 19.0 software by one-way analysis of variance, followed by the Tukey–Kramer post-hoc test, with the level of statistical significance set at $P < 0.05$.

Results and discussion

Characterisation of the CuHAP coating

The XRD patterns of pure and Cu-substituted HAP coatings are shown in Fig. 1A. In both of the patterns, typical HAP peaks (JCPDS No. 09-0432) were found to be the major phase, and no other unwanted peaks were found in the as-deposited coatings. Likewise, the XRD patterns of CuHAP were also nearly identical to HAP peaks with a sharp and intense peak at about $2\theta \approx 26°$. The same findings were reported in literature even with higher content of doped Cu^{2+} [10, 12]. Particularly, it was found that the position of CuHAP peak shifted slightly to higher angles from the standard XRD patterns for HAP (Fig. 1B). Cu^{2+} has ionic radius of 73 pm and is smaller than that of Ca^{2+} ions which is 100 pm; therefore, substitution of Ca^{2+} by Cu^{2+} ions leads to a contraction of the cell parameters of HAP [27]. The shift of the XRD peaks, with respect to the Cu-free HAP (JCPDS No. 09-0432), served as evidence of Cu substitution in obtained coatings [28].

The unit cell of HAP contains 10 Ca^{2+} ions in two different locations: the Ca(I) site, 4 cations connected with 9 oxygen atoms (Ca(I)–O distances: 0.241, 0.245, and 0.281 nm) and the Ca(II) site, 6 cations connected with 7 oxygen atoms (Ca(II)–O distances: 0.236, 0.239, and 0.251 nm) [29]. With a higher concentration of dopants, the incorporation of Ca^{2+} in the Ca(II) site is mostly preferred, as represented by the substitution with Zn^{2+}, Sr^{2+}, Pb^{2+}, and Cd^{2+}. However, with a lower concentration of dopants, the incorporation of Ca^{2+} in the Ca(I) site is more favorable [10]. In the present study, the concentrations of the dopants Cu^{2+} were low and it is supposed that the substitution of Ca^{2+} in the Ca(I) site was favorable.

FTIR spectra analysis was performed in order to examine the functional groups present in the as-deposited films. Figure 1C represents the FTIR spectra of CuHAP and HAP synthesized by ED. The spectral data for HAP, shown in Fig. 1C(a), distinctly showed the existence of various vibrational modes corresponding to hydroxyl and phosphate groups. The peaks at 3450 and 1635 cm^{-1}

Table 1 The amount of material needed to prepare 1000 ml of SBF

Order	Reagent	Purity (%)	Amount	Notes
1	DI water	N/A	400 ml	N/A
2	Sodium chloride (NaCl)	≥99.5	8.306 g	Reagents 1–6, including washings, were added individually, allowing enough time for each to fully dissolve between each addition
3	Sodium bicarbonate ($NaHCO_3$)	99.7–100.3	0.352 g	
4	Potassium chloride (KCl)	≥99.0	0.225 g	
5	Potassium phosphate dibasic trihydrate ($K_2HPO_4{\cdot}3H_2O$)	≥99.0	0.230 g	
6	Magnesium chloride hexahydrate ($MgCl_2{\cdot}6H_2O$)	≥99.0	0.311	
7	Hydrochloric acid (HCl)	1 M	40 ml	HCl was added in 5-ml amounts, and the solution pH was allowed to stabilise in between. Washings were also added
8	Calcium chloride ($CaCl_2$)	≥93.0	0.293	$CaCl_2$ was dissolved in 25 ml of DI water and added to solution, including washings
9	Sodium sulfate (Na_2SO_4)	≥99.0	0.072 g	Reagent 9 and washings were added
10	Tris-(hydroxymethyl)aminomethane ($(CH_2OH)_3CNH_2$)	≥99.8	6.063 g	TRIS was dissolved in 50 ml of DI water and added 5 ml at a time, allowing the pH to stabilise in between up to pH 7.45. HCl was then added to lower the pH to 7.42. TRIS was added up to pH 7.45 and this was repeated until all of the TRIS was added, including washings. Final pH was adjusted to 7.25 using HCl
11	HCl	1 M	Appropriate amount for pH adjustment	

corresponded to adsorbed H_2O on the surface of the prepared coatings. The peak at 3569 cm^{-1} was ascribed to the characteristic stretching vibrational mode of structural –OH groups. The peaks for the phosphate groups (PO_4^{3-}) were appeared at 569 and 599 cm^{-1} (υ_4), 962 cm^{-1} (υ_1), 1031, 1091 cm^{-1} (υ_3), and 468 cm^{-1} (υ_2), respectively. Particularly, the peaks at 1411 (υ_2) and 877 (υ_3) cm^{-1} could be attributed to CO_3^{2-} replacing the PO_4^{3-} in HAP, forming the B-type carbonated hydroxyapatite (CHAP) [30]. The CO_3^{2-} were from CO_2 in the air, which dissolved in the electrolyte solution ($CO_2 + H_2O = H_2CO_3$, $H_2CO_3 \rightarrow CO_3^{2-} + 2H^+$), and the B-type CHAP can normally be obtained from precipitation reaction [30]. The CO_3^{2-} can be detected up to 0.80 wt% in the HAP component of the bone mineral [30]. The existence of CO_3^{2-} is known to enhance both the solubility and the mechanical strength of HAP. Many researches have consistently revealed that CHAP typically shows superior bioactivity, cytocompatibility, and, if porous, osteoconduction in vivo [31–34]. The FTIR spectra shown in Fig. 1C(b) were similar to those reported for HAP. These spectra revealed the characteristic peaks of HAP. Not much manifest changes in the shapes and intensities of the peaks were detected for the CuHAP coating which suggest that no structural modification of HAP owing to the substitution of Cu was observed. This was in good agreement with reports introduced by Shanmugam et al. [11] in 2014 whose FTIR examination of the CuHAP did not provide confirmation of considerable change in the structure of the pure HAP.

The SEM micrographs of the electrodeposited HAP and Cu-doped HAP are shown in Fig. 2a–d. SEM results provide the direct information about the size and shape of the deposited coatings. The results suggested that the substitution of Cu in HAP increased the density, i.e., a relatively lower porosity than HAP coating. The presence of Cu^{2+} ions in the coating solution restrained the precipitation, resulting in a slight decrease of crystal size of doped HAP [19, 21]. According to the cross-sectional morphology of the as-deposited films shown in Fig. 2g, h, both HAP and CuHAP films formed smoothly and uniformly, with a thickness of nearly 10 μm without delamination and/or cracking at the interface. The thickness of 10 μm was suggested to be mostly preferred for bone deposition [19].

The EDS results of HAP coating are shown in Fig. 2e. The chemical composition consisted of Ca, P, Ti, and O. The Ca/P ratio was around 1.13, which was lower than 1.67 (the mole ratio of Ca to P of stoichiometric HAP). The EDS spectrum in Fig. 2f demonstrated the presence of Cu, Ca, P, Ti, and O. Notably, Ti was from the substrate, whereas the presence of Cu, Ca, P, and O was due to the surface coating of CuHAP. The Ca/P and Cu/P molar ratios were 1.04 and 0.026, respectively. Changes in the element to Ca^{2+} ratios revealed that Cu^{2+} was incorporated into the HAP crystal lattice by occupying the Ca^{2+} sites, which was

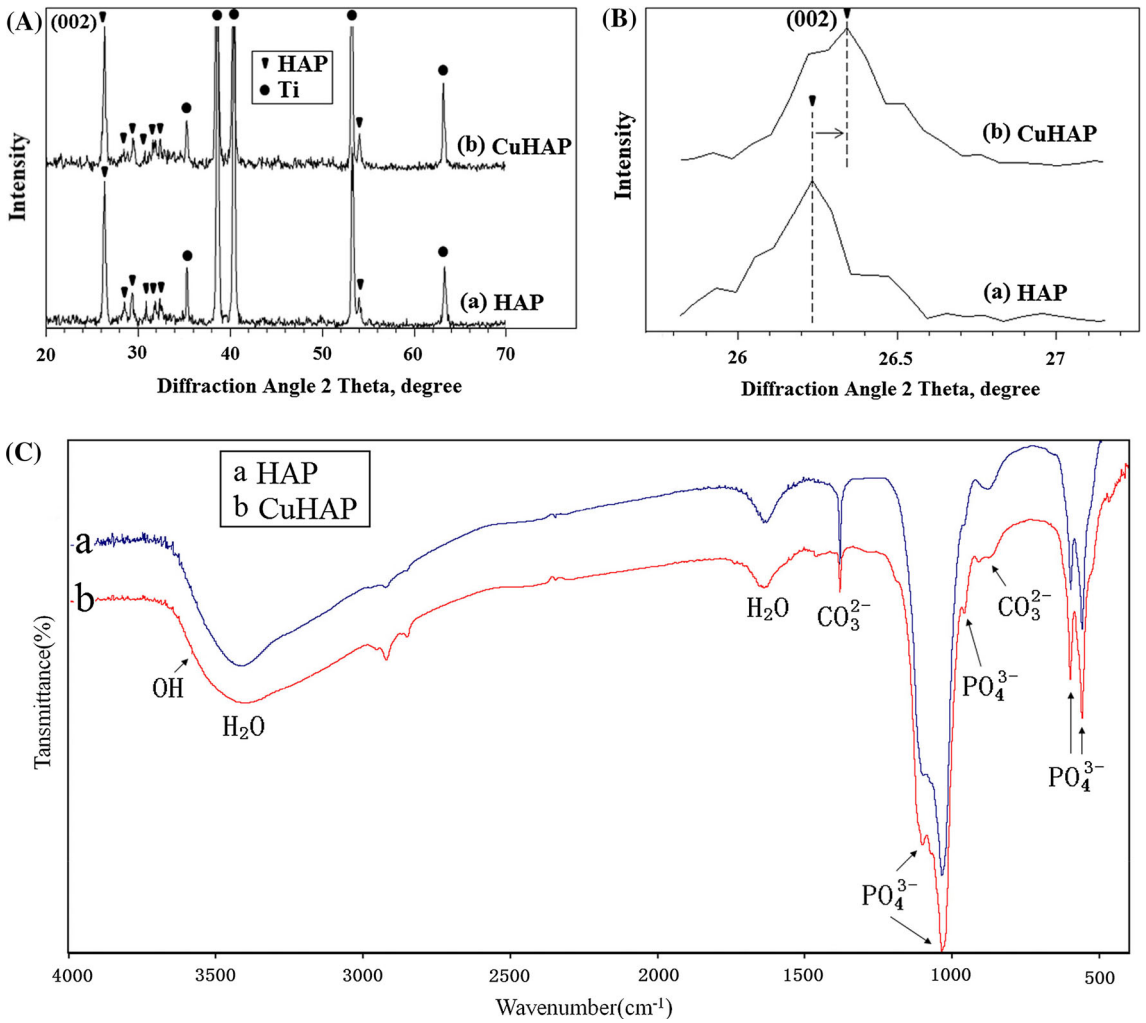

Fig. 1 **A** XRD patterns of HAP and CuHAP coatings on titanium; **B** partial magnification of the XRD patterns; **C** FTIR spectra of the deposits scraped from the Ti substrate

in accordance with earlier results [19, 21]. The above results suggest that CuHAP was Ca deficient with a few Cu substitution (about 0.80 wt%). The degree of Cu substitution x for CuHAP ($Ca_{10-x}Cu_x(PO_4)_6(OH)_2$) was about 0.025, according to the EDS results (Fig. 2f).

Figure 3 shows the mapping of the elements on the CuHAP coating surface. EDS elemental mapping demonstrated uniform distribution of Cu, Ca, P, Ti, and O on the structure surface. Evidently, the coating maintained a uniform and evenly distributed Cu across the entire surface.

Corrosion behavior

The potentiodynamic scan of the uncoated, electrodeposited HAP and CuHAP coatings on Ti substrate in SBF is shown in Fig. 4. The Tafel extrapolation method was employed to calculate the corrosion parameters such as corrosion potential (E_{corr}) and corrosion current density (i_{corr}) from the potentiodynamic curves. The results of these corrosion parameters are listed in the inset of Fig. 4. The curves of the specimens shifted to a nobler E_{corr} and a lower i_{corr}. The corrosion rate of a material proportional to the i_{corr} at a given potential, and materials with higher value of i_{corr} material will be more prone to corrosion [24].

The result of Tafel slope values reveals that i_{corr} of bare Ti in SBF is ($i_{corr} = 34.72$ μA, $E_{corr} = -0.902$ V) higher than that of the electrodeposited HAP ($i_{corr} = 16.77$ μA, $E_{corr} = -0.840$ V)- and CuHAP ($i_{corr} = 9.09$ μA, $E_{corr} = -0.811$ V)-coated Ti substrate. So, the analysis of Tafel slope values demonstrates that the CuHAP-coated Ti with lower i_{corr} values is more corrosion resistant than uncoated and HAP-coated Ti in SBF. The films restricted the penetration of the solution into the bulk substrate and thereby reduced the corrosive attack of chloride ions. The earlier corrosion study on ionic-doped HAP coatings shows the same kind of result [2]. Anawati et al. [35] have

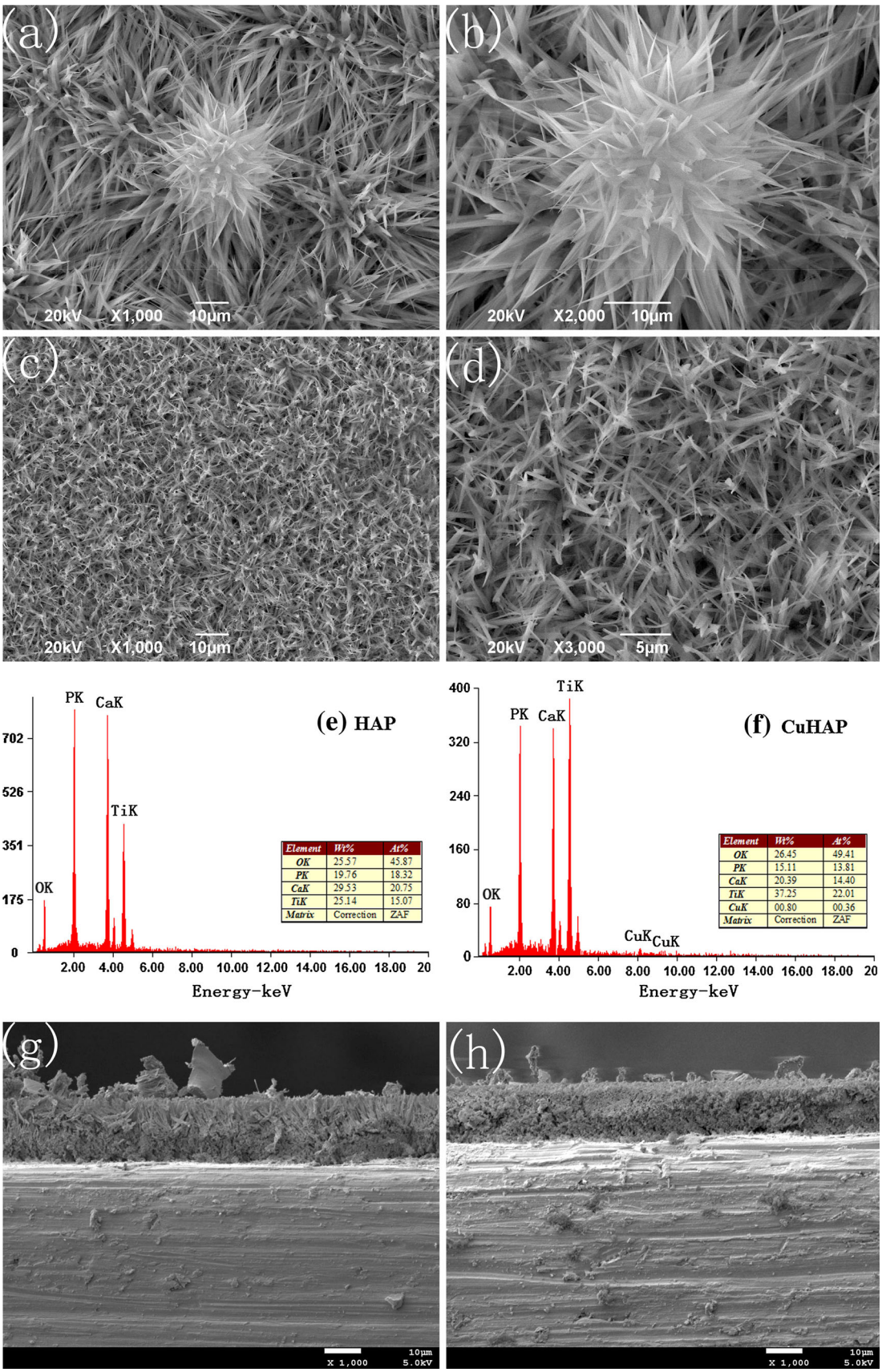
(a)
20kV X1,000 10μm
(b)
20kV X2,000 10μm
(c)
20kV X1,000 10μm
(d)
20kV X3,000 5μm
(e) HAP
PK CaK TiK OK
Element Wt% At%
OK 25.57 45.87
PK 19.76 18.32
CaK 29.53 20.75
TiK 25.14 15.07
Matrix Correction ZAF
Energy-keV
(f) CuHAP
TiK PK CaK OK CuK CuK
Element Wt% At%
OK 26.45 49.41
PK 15.11 13.81
CaK 20.39 14.40
TiK 37.25 22.01
CuK 00.80 00.36
Matrix Correction ZAF
Energy-keV
(g)
X 1,000 10μm 5.0kV
(h)
X 1,000 10μm 5.0kV

◀**Fig. 2** SEM images of the **a**, **b** HAP coating and the **c**, **d** CuHAP coating; EDS elemental spectrum of the **e** HAP coating and the **f** CuHAP coating; Cross-section morphology of the **g** HAP coating and the **h** CuHAP coating

suggested that coatings with open flaws, i.e., coatings with uncompressed structures such as HAP on Ti, allow free flow of species in the solution and liable access to O_2 which improves self-regeneration of protective oxide coatings and thereupon better corrosion protection. In the present study, decreased i_{corr} values suggest that the as-deposited HAP coating on Ti substrate hinders ionic and electronic transport at the coating/electrolyte interface and also facilitates self-regeneration of Ti substrate through its open flaws, which brings about corrosion protection of the substrate. The CuHAP coating was prepared on Ti substrate, consequently decreasing the specific surface, because a denser coating was formed, as proven by the SEM micrograph in Fig. 2. The reduced grain size has a distinguishing feature in elevating electron activity at the grain boundaries [19], thus decreasing i_{corr} which is equal to improved corrosion protection. These results illustrated that the CuHAP coating acted as a protective barrier layer, which avoided ion diffusion and offered corrosion protection for the Ti substrate.

Antimicrobial assessment

Since the antibiotics may not be effective for the infection on the surface of the Ti coated with HAP, the antibacterial agent like Cu is doped in HAP coating. The results of the quantitative antibacterial tests were presented in Fig. 5. Antimicrobial ratio (K) was calculated from the number of colonies after 24-h incubation periods and listed in the inset of Fig. 5. The CuHAP coating showed the highest activity against the *E. coil* compared to HAP coating and the control. The antimicrobial results revealed that Cu ions released from CuHAP have strong bactericidal effect against these organisms (antimicrobial ratio >75 %)

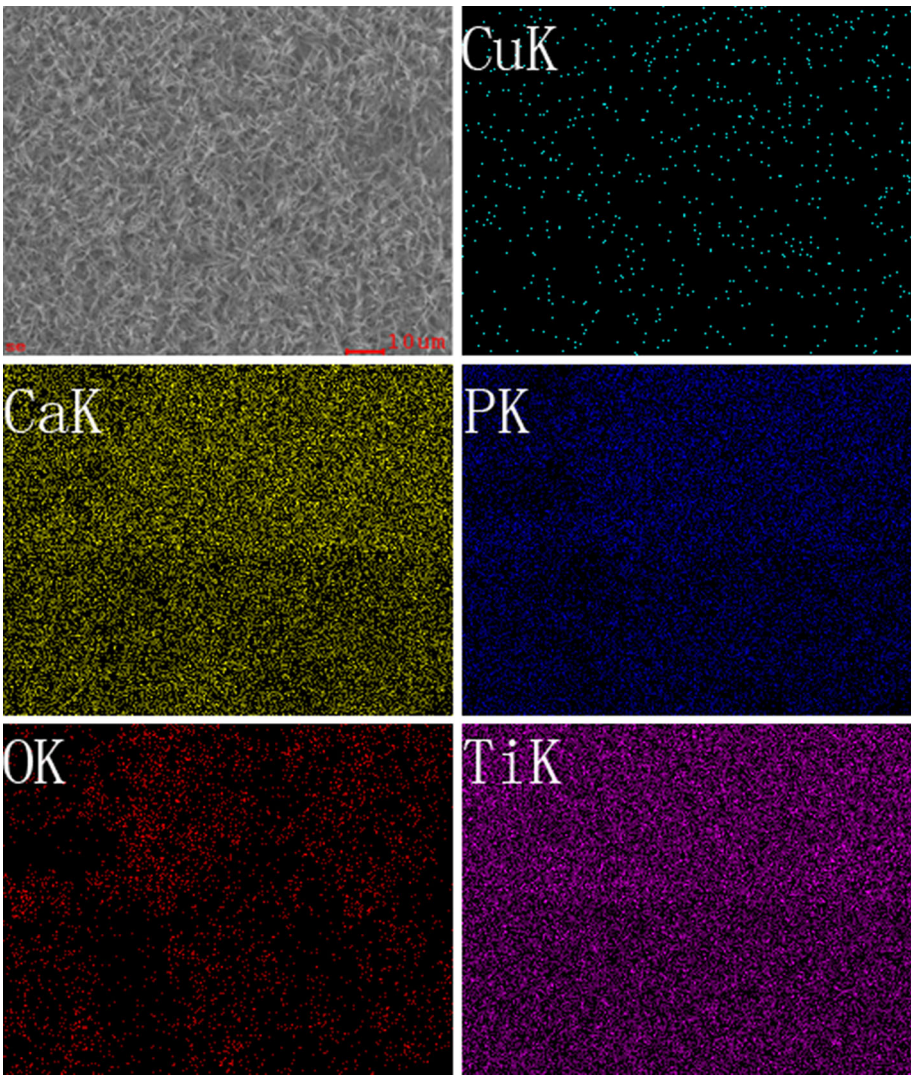

Fig. 3 Elemental mapping images of the CuHAP coating surface

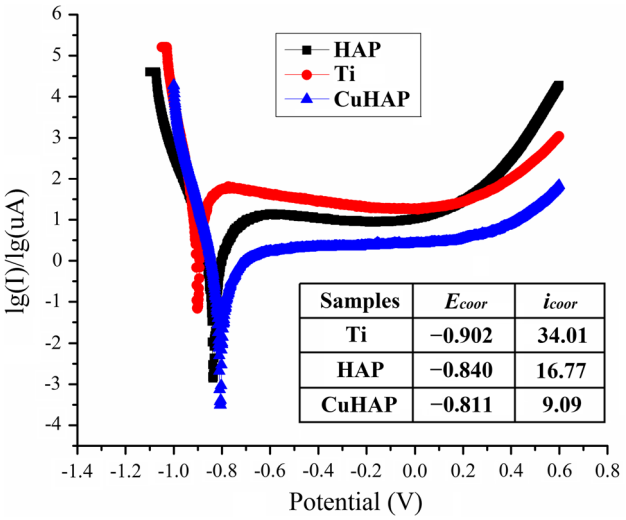

Fig. 4 The polarisation curves of the bare Ti and the Ti coated with coatings in SBF

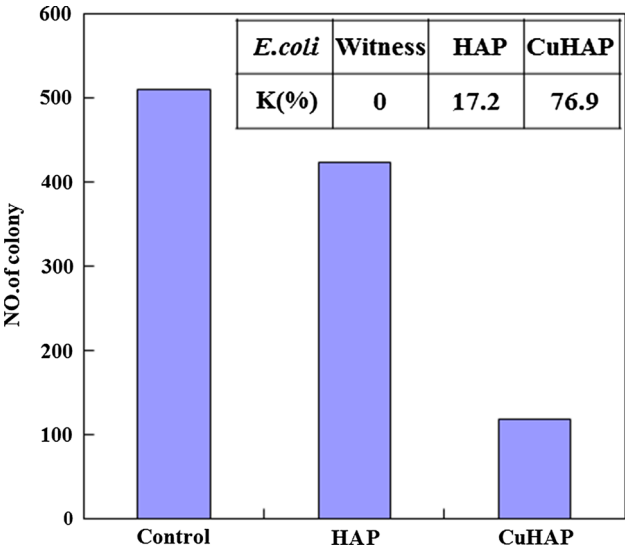

Fig. 5 Antimicrobial activity of the HAP and CuHAP coatings

(Fig. 5). This indicated the effect of substitution of Cu in HAP on the antimicrobial activity.

Several recent investigations research antimicrobial activity and cytocompatibility of Cu-doped hydroxyapatite [36]. Li et al. [12] prepared CuHAP using the ion exchange method. This biomaterial was effectively bactericidal against *E. coli* but cytotoxic to human fetal osteoblast cells. The preparation of Cu^{2+}-doped HAP using a neutralization technique was performed by Stanic et al. [36]. Their examination confirmed that Cu^{2+}-HAP had a number reduction ability of viable cells against *E. coli*, *S. aureus*, and Candida albicans. Some of the recent studies introduce the mechanism of antimicrobial activity of the materials that involve Cu(II) ions. Du et al. [37] have suggested that the chitosan nanoparticles-loaded Cu(II) ions interact with bacterial cell membranes of *E. coli*, causing structural changes and, eventually, cell death. Nan et al. [38] also suggested that the structure of the outer cell membrane responsible for the cell permeability was greatly changed for the *E. coli*, after being in contact with the antimicrobial stainless steel involving Cu(II) ions, indicating that cell walls were badly undermined and a lot of contents in the cells were released. Ohsumi et al. [39] suggested that Cu(II) caused selective lesions of the permeability barrier of the plasma membrane of *S. cerevisiae*, but did not affect the permeability of the vacuolar membrane.

In vitro bioactivity responses

One of the efficient parameters in researching the bioactivity of the biomaterials was to study the precipitation behavior of bone-like apatites in the SBF. Figure 6a, b shows the surface views of the as-deposited coatings after being soaked in the SBF for 10 d. In Fig. 6a, it can be seen that the surface of the HAP coating was completely covered by mountain-like crystals of the apatite-like precipitations. The surface morphology was different from that of the CuHAP coating, that the surface presented a semi-spherical appearance of apatite-like precipitations (Fig. 6b). This difference in the surface morphology could be caused by the existence of Cu in the CuHAP coating, which decreased the bio-absorbability of phosphates in the SBF. The bioactivity process will occur at the material periphery through the releasing and adsorbing ions. Thus, different coatings show different morphologies of the precipitated apatites. The XRD patterns of the HAP and CuHAP coatings after being soaked in SBF were given in Fig. 6c, d, that typical apatite peaks were identified in both patterns. The above-mentioned results indicated that the CuHAP coating can successfully induce apatite nucleation and growth on Ti surface after soaking in SBF. Recently, the investigation is still open on the true significance of in vitro assays. Indeed, the SBF is pure saline solutions and, since it does not include cells, it is not able to reproduce the true complexity of a physiological environment [40]. However, it is generally accepted that SBF assays may be useful to assess the capability to facilitate the growth of a HCAP surface layer, which is close to the mineral composition of human bone [30]. So, even though the apatite-forming ability does not effectively suggest the bone-bonding ability [41], the development of a HCAP layer in SBF may be still considered a favorable indicator of the inclination to sustain the mineralization process [42]. Numerous investigations have reported the bioactivity of HAP in vivo [42], which extremely indicates that the growth of apatite appeared on the surface of specimens soaked in SBF is a real positive result. The results of the

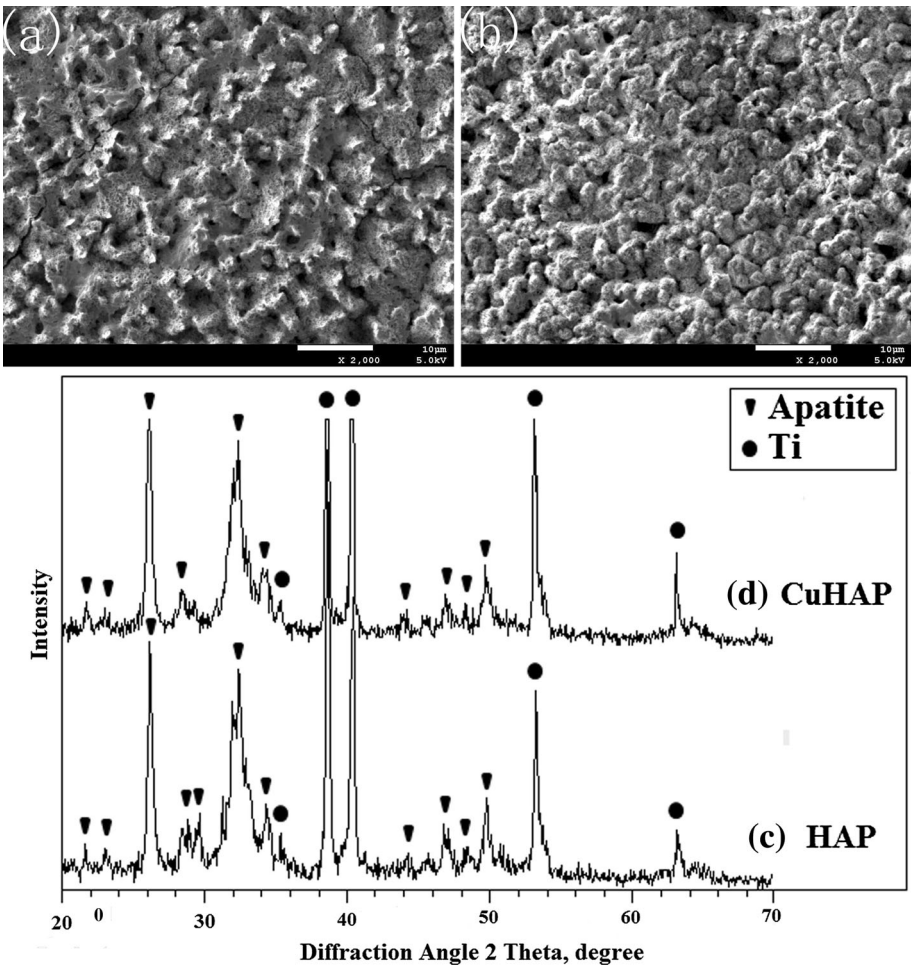

Fig. 6 SEM image of the **a** HAP coating and the **b** CuHAP coating after immersion in SBF for 10 d; XRD patterns of the **a** HAP coating and the **b** CuHAP coating after immersion in SBF for 10 d

SBF tests therefore suggest that the CuHAP-covered Ti had superior in vitro bioactivity. Nevertheless, this is only a preliminary test since cell assays are essential to assess the in vitro cytocompatibility of the topcoat as follows.

In vitro cytotoxicity studies with MC3T3-E1 cells

SEM images revealed differences in cell density and spreading patterns among the MC3T3-E1 cells grown on the HAP-coated and non-coated Ti substrates after 24 h (Fig. 7). The results indicated that the cells spread well onto all the samples and exhibit active cytoskeletal extension. This appearance suggested good cell viability on the CuHAP and HAP films. As shown in Figure 7c–f, the cell viability of 0.8 wt% CuHAP showed cell morphology similar to the HAP which declares that this does not show any toxic nature. Therefore, it could be concluded that Cu(II) does not affect the cell morphology of MC3T3-E1 cells. Interestingly, on the bare Ti surface (Fig. 7a, b), the cell density was similar to that on the apatite-coated specimens, manifesting that all the three samples showed sufficiently high cell viability after 24 h of incubation.

In the present work, the cytotoxicity of CuHAP coating was evaluated by the MTT test using the MC3T3-E1 as a cell model. The HAP coatings are designed as a control group because HAP has been confirmed to have superior cytocompatibility and bioactivity [43, 44]. From the MTT tests (Fig. 8), it is distinct that the number of cells proliferated with time for all samples. After 1 day of culturing, the cell number did not significantly differ between the pure Ti and the coated specimens (CuHAP and HAP coatings), which was in agreement with the cell adhesion results (Fig. 7). With increasing culture time, cell proliferation became apparent for all samples. During the following two periods (3 and 5 d), the cell numbers on bare Ti were significantly lower ($P < 0.05$) than those on the coated specimens, indicating that the CuHAP and HAP coatings had higher cytocompatibility than the bare Ti. Cell proliferation activity of MC3T3-E1 cultured on the CuHAP and HAP coatings showed no notable differences ($P < 0.05$) after culturing for 3 and 5 d. However, there was a slight trend of increased proliferation activity in a Cu-content-dependent manner after culturing for 5 d. These results showed that the obtained HAP coating doped with

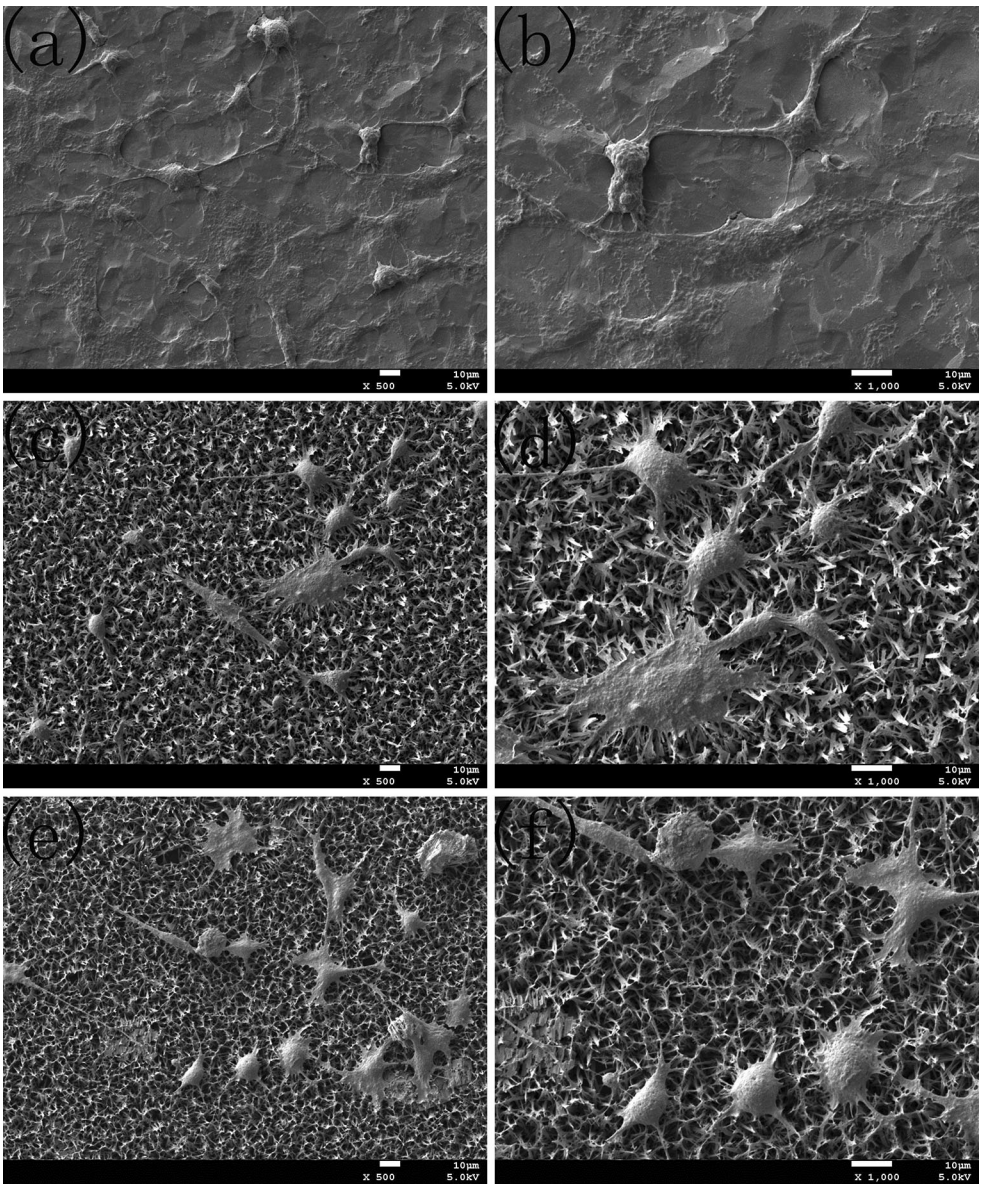

Fig. 7 SEM morphologies of the MC3T3-E1 cells grown on bare Ti substrate (**a**), HAP coating (**c**) and CuHAP coating (**e**); The higher magnification images of the surface of the MC3T3-E1 cells grown on bare Ti substrate (**b**), HAP coating (**d**) and CuHAP coating (**f**)

the lower content of Cu^{2+} (0.80 wt%) showed good cytocompatibility and had no noticeable cytotoxicity toward osteoblast cells, and was favorable for implant applications. But, such concentration of Cu must also instill an antibacterial effect by restraining the growth of bacteria to prevent the microbial infections when used as in vivo implants.

It is critical that the target coating surface does not release any toxic ions or compounds that could injure the cells involved in osteogenesis. In this case, HAP, the main component of the hard tissue, releases minimal toxicity to the cells of the guest organism. Cu ions may be useful in vitro to promote angiogenesis prior to implantation; therefore, stimulating the survival of cells is incorporated in tissue engineering equipment [45–47]. It is well known that Cu missing causes thinning and instability of bone tissue due to decreased osteogenesis [48]. Cu has been shown to reduce osteogenic differentiation of mesenchymal stem cells after 14 days [49]. In addition, it was shown that a lack of Cu leads to a reduction of bone strength in rats [50]. Even if it is known that Cu plays a role in bone formation and angiogenesis, not all involved mechanisms are well understood yet. The complex of Cu with glycylhistidyllysine tripeptide (GHK) has been illustrated to facilitate both angiogenesis in vivo and osteoblasts proliferation and attachment [51]. Radovanovic et al. [10]

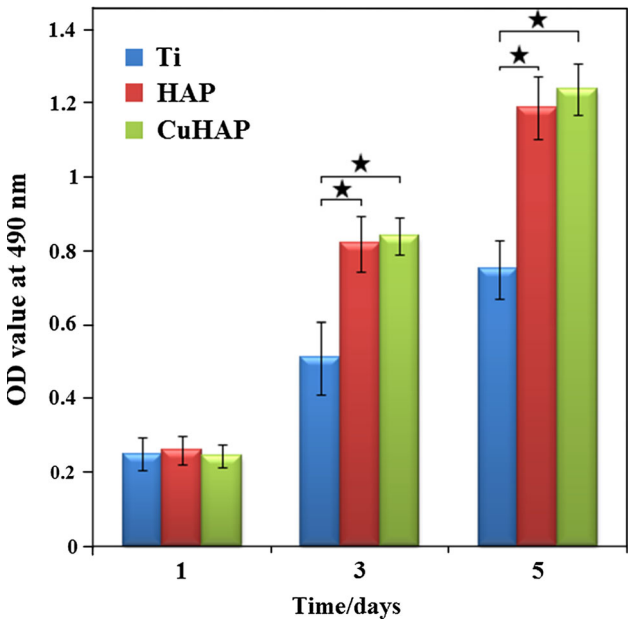

Fig. 8 OD measurements illustrating MC3T3-E1 cell proliferation on the ceramic coatings and bare Ti substrate after culturing for 1, 3, and 5 d (one-way ANOVA, *black star*, $p < 0.05$)

suggested that the low concentration of released Cu ions offered good antimicrobial activity against *S. aureus*, *E. coli*, *Ps. Aeruginosa*, and *C. albicans* for Cu-doped HAP, and, simultaneously, the CuHAP was not cytotoxic, as was obvious from MTT tests. Gbureck et al. [52] studied the in vitro effect of Cu on the growth and activity of osteoblasts (MG 63) seeded on brushite scaffolds as well as on glass disks. The results reveal that Cu(II) improves cell activity and proliferation of osteoblasts on calcium phosphate cements and moreover affects the expression of several special osteogenic protein such as bone sialoprotein or osteocalcin. Therefore, the modification of calcium phosphate cements with Cu may provide a likely alternative to protein-based modification to promote cell viability for a superior bone healing.

Bone formation comprises three stages: adhesion, proliferation, and differentiation. Topography plays an important role in the first step, while the chemical properties of the surface contribute to the proliferation and differentiation steps [45]. Cell proliferation and adhesion was influenced by the surface properties of biomaterial, including surface roughness, wettability, morphology, and chemistry [53]. Generally, a rough surface could stimulate osteoblast proliferation during the osteointegration process [53]. In this study, SEM results demonstrated that the mean roughness of the control HAP layer was larger than that of the CuHAP coating. However, after 5 days of cell culture, the CuHAP coating revealed superior cell viability than the control (Ti) and a little difference compared with HAP (Fig. 8). This meant that Cu release or the presence of Cu in the CuHAP coating may play an even more important role in promoting cell growth than roughness, because Cu release may promote cell viability and the presence of Cu may alter the surface potential to enhance cell attachment.

CHAP is a superior biomaterial since CHAP is very similar to the human hard tissue. As compared with HAP, CHAP has superior biocompatibility, osteoconductivity, bone-bonding ability, and cell adhesion and proliferation [31]. Melville et al. [33] found an equal or even better cell adhesion and proliferation on sintered CHAP compared to a HAP reference. Ilse Pieters et al. [32] also found that the potential of biomimetic apatites with a carbonate content higher than 11 % supported high cell adhesion and proliferation of MC3T3-E1. Landi et al. [34] studied the proliferation and differentiation of mesenchymal stem cells (MSCs) and human osteoblasts (MG-63) on CO_3^{2-}, Mg co-doped HAP (MCHAP), and suggested that MCHAP was found to be a favorable substrate for attachment and proliferation of MG-63 as well as for MSCs. The incorporation of CO_3^{2-} groups would generate a more dynamic reactive surface, which is a good omen for the resorbable nature of CHAP in vivo. Moreover, it has been reported that calcium ions (Ca^{2+}) in CuHAP coatings form locations of positive charges which help the adsorption of vitronectin and fibronectin [54], which are the two major proteins affecting cell adhesion and spreading [55]. All of the above analyses suggested that the as-deposited carbonated CuHAP coating has the potential to decrease bacterial adhesion to the surface of Ti implants while maintaining the healthy osteoblast cellular activity.

Conclusions

In this study, ED was successfully used for the synthesis of Cu-substituted carbonated hydroxyapatite coating, which had good antibacterial efficacy and corrosion resistance, and no cytotoxicity. The CuHAP coating was uniform and carbonated with a few Cu incorporations. The doping of Cu^{2+} into HAP slightly reduced the porosity, and the coating became denser. The CuHAP film exhibited higher corrosion resistance in SBF than the HAP coating. SBF immersion tests revealed that CuHAP-coated Ti had favorable in vitro bioactivity. The in vitro biocompatibility and antibacterial tests suggested that the low concentration of released Cu ions provided satisfactory antimicrobial activity against *E. coli* for Cu-doped HAP, simultaneously, the CuHAP was not cytotoxic, as was obvious from MTT tests. Thus, the as-prepared CuHAP coating will serve as a better candidate for biomedical applications with good antibacterial property and bone-bonding ability.

Acknowledgement This work was supported by the National Basic Research Program of China ("973" Program, No. 2011CB503700) and the outstanding doctoral academic projects of the University of Electronic Science and Technology of China (No. YBXSZC201 31042).

References

1. Mohseni E, Zalnezhad E, Bushroa AR (2014) Comparative investigation on the adhesion of hydroxyapatite coating on Ti–6Al–4V implant: a review paper. Int J Adhes Adhes 48:238–257
2. Gopi D, Ramya S, Rajeswari D, Surendiran M, Kavitha L (2014) Development of strontium and magnesium substituted porous hydroxyapatite/poly(3,4-ethylenedioxythiophene) coating on surgical grade stainless steel and its bioactivity on osteoblast cells. Colloid Surf B 114:234–240
3. de Souza ID, Cruz MAE, de Faria AN, Zancanela DC, Simão AMS, Ciancaglini P et al (2014) Formation of carbonated hydroxyapatite films on metallic surfaces using dihexadecyl phosphate–LB film as template. Colloid Surf B 118:31–40
4. Rau JV, Cacciotti I, De Bonis A, Fosca M, Komlev VS, Latini A et al (2014) Fe-doped hydroxyapatite coatings for orthopedic and dental implant applications. Appl Surf Sci 307:301–305
5. Kaygili O, Dorozhkin SV, Keser S (2014) Synthesis and characterization of Ce-substituted hydroxyapatite by sol–gel method. Mater Sci Eng C 42:78–82
6. Gopi D, Ramya S, Rajeswari D, Karthikeyan P, Kavitha L (2014) Strontium, cerium co-substituted hydroxyapatite nanoparticles: synthesis, characterization, antibacterial activity towards prokaryotic strains and in vitro studies. Colloid Surf A 451:172–180
7. Mocanu A, Furtos G, Rapuntean S, Horovitz O, Flore C, Garbo C et al (2014) Synthesis; characterization and antimicrobial effects of composites based on multi-substituted hydroxyapatite and silver nanoparticles. Appl Surf Sci 298:225–235
8. Shanmugam S, Gopal B (2014) Synthesis; antimicrobial and cytotoxicity evaluation of aliovalent substituted hydroxyapatite. Appl Surf Sci 303:277–281
9. Gopi D, Shinyjoy E, Kavitha L (2014) Synthesis and spectral characterization of silver/magnesium co-substituted hydroxyapatite for biomedical applications. Spectrochim Acta A 127:286–291
10. Radovanovic Z, Jokic B, Veljovic D, Dimitrijevic S, Kojic V, Petrovic R et al (2014) Antimicrobial activity and biocompatibility of Ag^{+}- and Cu^{2+}-doped biphasic hydroxyapatite/α-tricalcium phosphate obtained from hydrothermally synthesized Ag^{+}- and Cu^{2+}-doped hydroxyapatite. Appl Surf Sci 307:513–519
11. Shanmugam S, Gopal B (2014) Copper substituted hydroxyapatite and fluorapatite: synthesis, characterization and antimicrobial properties. Ceram Int 40:15655–15662
12. Li Y, Ho J, Ooi CP (2010) Antibacterial efficacy and cytotoxicity studies of copper(II) and titanium(IV) substituted hydroxyapatite nanoparticles. Mater Sci Eng C 30:1137–1144
13. Erol MM, Mourino V, Newby P, Chatzistavrou X, Roether JA, Hupa L et al (2012) Copper-releasing, boron-containing bioactive glass-based scaffolds coated with alginate for bone tissue engineering. Acta Biomater 8:792–801
14. Habibovic P, Barralet JE (2011) Bioinorganics and biomaterials: bone repair. Acta Biomater 7:3013–3026
15. Pei XB, Zeng YX, He R, Li ZJ, Tian LY, Wang J et al (2014) Single-walled carbon nanotubes/hydroxyapatite coatings on titanium obtained by electrochemical deposition. Appl Surf Sci 295:71–80
16. Kim HJ, Jeong YH, Choe HC, Brantley WA (2014) Surface characteristics of hydroxyapatite coatings on nanotubular Ti–25Ta–xZr alloys prepared by electrochemical deposition. Surf Coat Technol. doi:10.1016/j.surfcoat.2014.03.013
17. Sun GF, Ma J, Zhang SM (2014) Electrophoretic deposition of zinc-substituted hydroxyapatite coatings. Mater Sci Eng C 39:67–72
18. Zhang LL, Li HJ, Li KZ, Zhang SY, Fu QG, Zhang YL et al (2014) Preparation and characterization of carbon/SiC nanowire/Na-doped carbonated hydroxyapatite multilayer coating for carbon/carbon composites. Appl Surf Sci 313:85–92
19. Huang Y, Ding QQ, Han SG, Yan YJ, Pang XF (2014) Characterisation, corrosion resistance and in vitro bioactivity of manganese-doped hydroxyapatite films electrodeposited on titanium. J Mater Sci Mater Med 24:1853–1864
20. Huang Y, Yan YJ, Pang XF (2013) Electrolytic deposition of fluorine-doped hydroxyapatite/ZrO_2 films on titanium for biomedical applications. Ceram Int 39:245–253
21. Huang Y, Yan YJ, Pang XF, Ding QQ, Han SG (2013) Bioactivity and corrosion properties of gelatin-containing and strontium-doped calcium phosphate composite coating. Appl Surf Sci 282:583–589
22. Yan YJ, Ding QQ, Huang Y, Han SG, Pang XF (2014) Magnesium substituted hydroxyapatite coating on titanium with nanotublar TiO_2 intermediate layer via electrochemical deposition. Appl Surf Sci 305:77–85
23. Yan YJ, Zhang XJ, Huang Y, Ding QQ, Pang XF (2013) Antibacterial and bioactivity of silver substituted hydroxyapatite/TiO_2 nanotube composite coatings on titanium. Appl Surf Sci 282:583–589
24. Yusoff MFM, Kadir MRA, Iqbal N, Hassan MA, Hussain R (2014) Dipcoating of poly (ε-caprolactone)/hydroxyapatite composite coating on Ti6Al4V for enhanced corrosion protection. Surf Coat Technol 245:102–107
25. Goudarzi M, Batmanghelich F, Afshar A, Dolati A, Mortazavi G (2014) Development of electrophoretically deposited hydroxyapatite coatings on anodized nanotubular TiO_2 structures: corrosion and sintering temperature. Appl Surf Sci 301:250–257
26. Kokubo T, Takadama H (2006) How useful is SBF in predicting in vivo bone bioactivity? Biomaterials 27:2907–2915
27. Batra U, Kapoor S, Sharma S (2012) Influence of magnesium ion substitution on structural and thermal behavior of nanodimensional hydroxyapatite. J Mater Eng Perform 22:1798–1806
28. Hu W, Ma J, Wang JG, Zhang SM (2012) Fine structure study on low concentration zinc substituted hydroxyapatite nanoparticles. Mater Sci Eng C 32:2404–2410
29. Ellis DE, Terra J, Warschkow O, Jiang M, González GB, Okasinski JS et al (2006) A theoretical and experimental study of lead substitution in calcium hydroxyapatite. Phys Chem Phys 28:967–976
30. Zhang LL, Li HJ, Li KZ, Fu QG, Zhang YL, Liu SJ (2014) A Na and Si co-substituted carbonated hydroxyapatite coating for carbon nanotubes coated carbon/carbon composites. Ceram Int 40:13123–13130
31. Rakmae S, Ruksakulpiwat Y, Sutapun W, Suppakarn N (2012) Effect of silane coupling agent treated bovine bone based carbonated hydroxyapatite on in vitro degradation behavior and bioactivity of PLA composites. Mater Sci Eng C 32:1428–1436
32. Pieters IY, Van den Vreken NMF, Declercq HA, Cornelissen MJ, Verbeeck RMH (2010) Carbonated apatites obtained by the hydrolysis of monetite: influence of carbonate content on adhesion and proliferation of MC3T3-E1 osteoblastic cells. Acta Biomater 6:1561–1568
33. Melville AJ, Harrison J, Gross KA, Forsythe JS, Trounson AO, Mollard R (2006) Mouse embryonic stem cell colonization of carbonated apatite surfaces. Biomaterials 27:615–622
34. Landi E, Tampieri A, Mattioli-Belmonte M, Celotti G, Sandri M, Gigante A, Fava P et al (2006) Biomimetic Mg- and Mg,

CO_3-substituted hydroxyapatites: synthesis, characterization and in vitro behavior. J Eur Ceram Soc 26:2593–2601
35. Anawati H, Tanigawa H, Asoh T, Ohno M, Ono Kubota S (2013) Electrochemical corrosion and bioactivity of titanium–hydroxyapatite composites prepared by spark plasma sintering. Corros Sci 70:212–220
36. Stanic V, Dimitrijevic S, Antic-Stankovic J, Mitric M, Jokic B, Plecas IB, Raicevic S (2010) Synthesis, characterization and antimicrobial activity of copper and zinc-doped hydroxyapatite nanopowders. Appl Surf Sci 256:6083–6089
37. Du WL, Xu YL, Xu ZR, Fan CL (2008) Preparation, characterization and antibacterial properties against *E. coli* K88 of chitosan nanoparticle loaded copper ions. Nanotechnology 19:085707
38. Nan L, Liu Y, Lü M, Yang K (2008) Study on antibacterial mechanism of copper bearing austenitic antibacterial stainless steel by atomic force microscopy. J Mater Sci Mater Med 19:3057–3062
39. Ohsumi Y, Kitamoto K, Anraku Y (1988) Changes induced in the permeability barrier of the yeast plasma membrane by cupric ion. J Bacteriol 170:2676–2682
40. Cattini A, Bellucci D, Sola A, Pawłowski L, Cannillo V (2014) Functional bioactive glass topcoats on hydroxyapatite coatings: analysis of microstructure and in vitro bioactivity. Surf Coat Technol 240:110–117
41. Pan H, Zhao X, Darvell BW, Lu WW (2010) Apatite–formation ability–predictor of "bioactivity"? Acta Biomater 6:4181–4188
42. Cox SC, Jamshidi P, Grover LM, Mallick KK (2014) Preparation and characterisation of nanophase Sr, Mg, and Zn substituted hydroxyapatite by aqueous precipitation. Mater Sci Eng C 35:106–114
43. Guo YJ, Long T, Chen W, Ning CQ, Zhu ZA, Guo YP (2013) Bactericidal property and biocompatibility of gentamicin-loaded mesoporous carbonated hydroxyapatite microspheres. Mater Sci Eng C 33:3583–3591
44. Costa DO, Prowse PDH, Chrones T, Sims SM, Hamilton DW, Rizkalla AS et al (2013) The differential regulation of osteoblast and osteoclast activity by surface topography of hydroxyapatite coatings. Biomaterials 34:7215–7226
45. Li CF, Ge XL, Zhao JY, Li GC, Bai JH, Du QY et al (2014) Preparation and characterization of novel hydroxyapatite/copper assemblies with well-defined morphologies. Solid State Sci 29:66–74
46. Gerard C, Bordeleau LJ, Barralet J, Doillon CJ (2010) The stimulation of angiogenesis and collagen deposition by copper. Biomaterials 31:824–831
47. Bi LX, Rahaman MN, Day DE, Brown Z, Samujh C, Liu X, Mohammadkhah A et al (2013) Effect of bioactive borate glass microstructure on bone regeneration, angiogenesis, and hydroxyapatite conversion in a rat calvarial defect model. Acta Biomater 9:8015–8026
48. Marie PJ (2010) The calcium-sensing receptor in bone cells: a potential therapeutic target in osteoporosis. Bone 46:571–576
49. Luthen F, Bergemann C, Bulnheim U, Prinz C, Neumann H-G, Podbielski A et al (2010) A dual role of Copper on the surfaces of bone implants. Mater Sci Forum 638–642:600–605
50. Jonas J, Burns J, Abel EW, Cresswell MJ, Strain JJ, Paterson CR (1993) Impaired mechanical strength of bone in experimental copper deficiency. Ann Nutr Metab 37:245–252
51. Pickart L (2008) The human tri-peptide GHK and tissue remodeling. J Biomater Sci Polym Ed 19:969–988
52. Ewald A, Kappel C, Vorndran E, Moseke C, Gelinsky M, Gbureck U (2012) The effect of Cu(II)-loaded brushite scaffolds on growth and activity of osteoblastic cells. J Biomed Mater Res A 100A:2392–2400
53. Tian B, Tang S, Li Y, Long T, Qu XH, Yu DG et al (2014) Fabrication, characterization, and biocompatibility of ethyl cellulose/carbonated hydroxyapatite composite coatings on Ti6Al4V. J Mater Sci Mater Med 25:2059–2068
54. Rad AT, Solati-Hashjin M, Osman NAA, Faghihi S (2014) Improved bio-physical performance of hydroxyapatite coatings obtained by electrophoretic deposition at dynamic voltage. Ceram Int 40:12681–12691
55. Webster TJ, Ergun C, Doremus RH, Siegel RW, Bizios R (2000) Specific proteins mediate enhanced osteoblast adhesion on nanophase ceramics. J Biomed Mater Res 51:475–483